Electrochemical Nitrate Reduction to Ammonia Using Laser Processed Nb_2AlC: The Role of Effective Al Etching

Shaista Nouseen [a,b], Sujit Deshmukh [b], Michal Langer,[c] Michal Otyepka,[c,d] Martin Pumera [a,b,e,f,g*]

[a] Quantum Materials Laboratory, 3D Printing & Innovation Hub, Center for Nanorobotics and Machine Intelligence, Department of Chemistry and Biochemistry, Mendel University in Brno, Zemedelska 1, Brno 61300, Czech Republic

[b] Future Energy and Innovation Laboratory, Central European Institute of Technology, Brno University of Technology, Purkynova 123, Brno 61200, Czech Republic

[c]IT4Innovations, VSB – Technical University of Ostrava, 17. listopadu 2172/15, Ostrava-Poruba 70800, Czech Republic

[d]Czech Advanced Technology and Research Institute (CATRIN), Regional Centre of Advanced Technologies and Materials, Palacký University Olomouc, Šlechtitelů 27, Olomouc, 77900, Czech Republic

[e] Advanced Nanorobots and Multiscale Robotics Laboratory, Faculty of Electrical Engineering and Computer Science, VSB - Technical University of Ostrava, 17. listopadu 2172/15, Ostrava 70800, Czech Republic

[f]Department of Medical Research, China Medical University Hospital, China Medical University, No. 91 Hsueh-Shih Road, Taichung, Taiwan

[g]Department of Chemical and Biomolecular Engineering, Yonsei University, 50 Yonsei-ro, Seodaemun-gu, Seoul, 03722, Korea

Corresponding Author

*Email: pumera.research@gmail.com

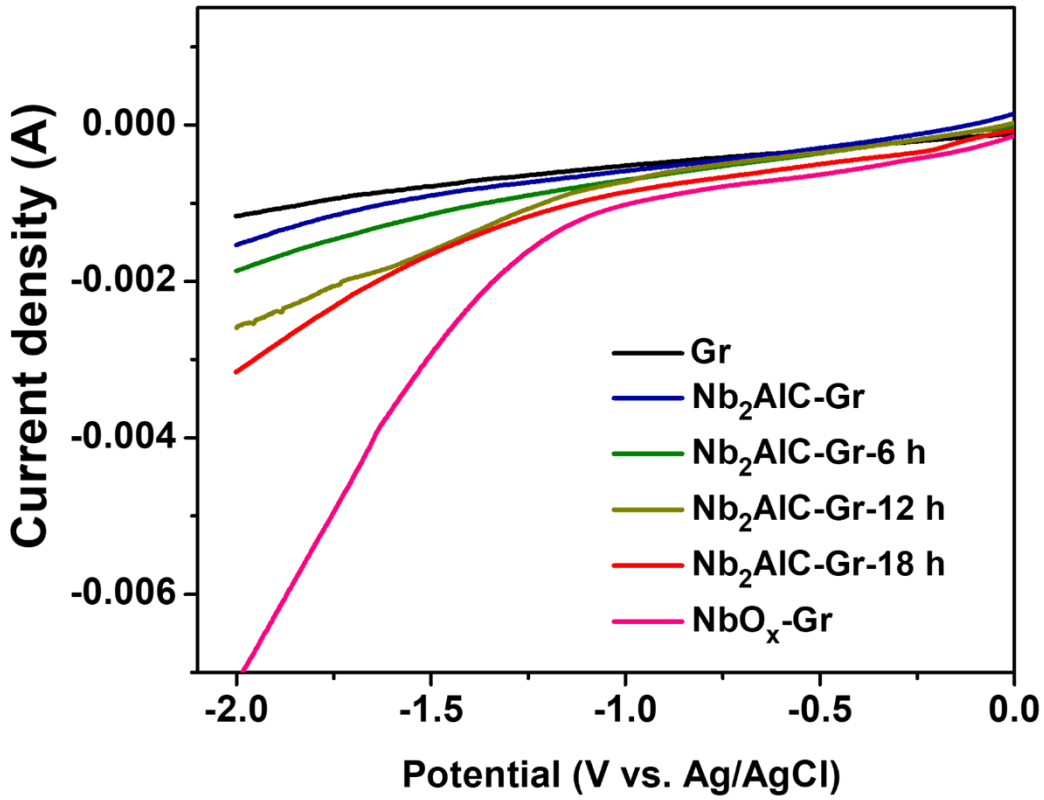

Figure S1. Linear sweep voltammetry measurement of Gr, Nb_2AlC-Gr, and in-situ electrochemically etched electrodes Nb_2AlC-Gr-6 h, Nb_2AlC-Gr-12 h, Nb_2AlC-Gr-18 h, and NbO_x-Gr.

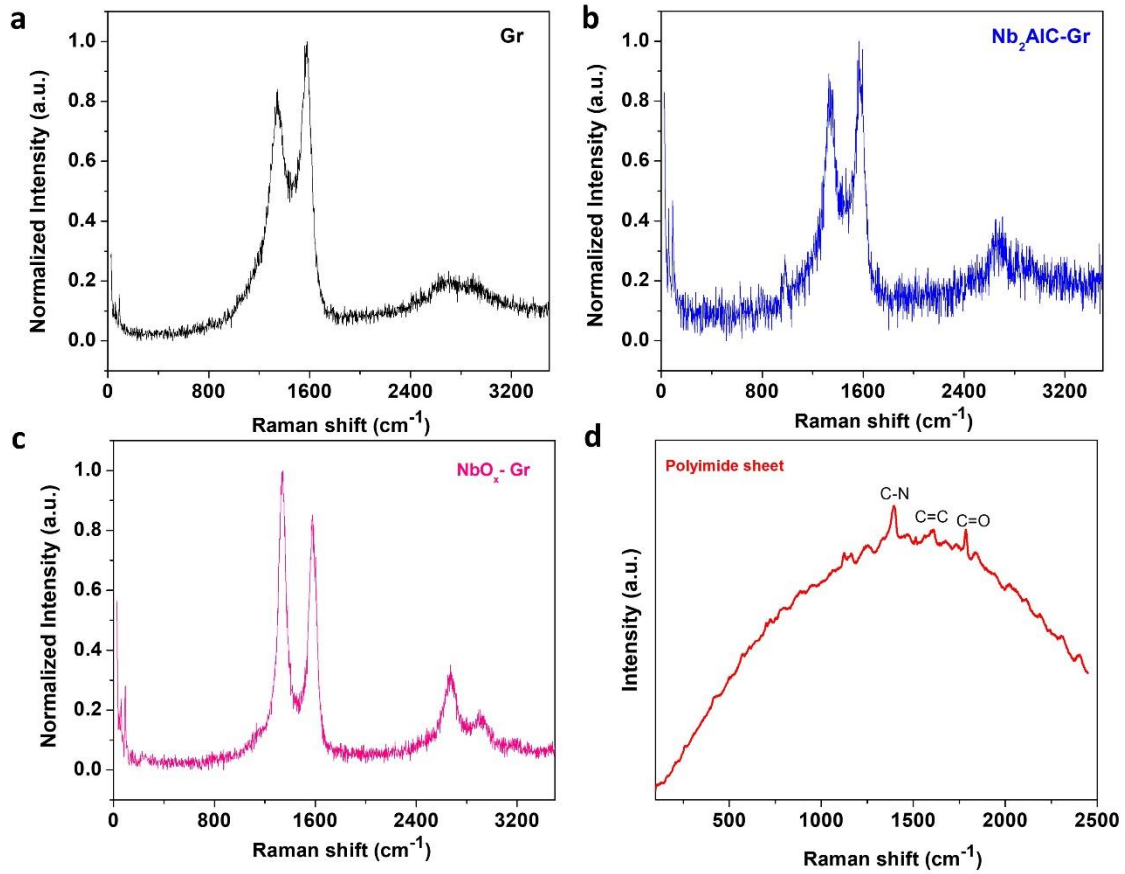

Figure S2. Raman spectra for (a) Gr, (b) Nb_2AlC-Gr, (c) NbO_x-Gr electrodes and (d) pristine polyimide sheet.

Coherence length calculation: The coherence length (L_a) is determined utilizing the equation (1), which determines the structure order along *ab* planes.[1]

$$L_a\ (nm) = (2.4*10^{-10}) * \lambda^4_{nm}\ (I_G/I_D) \qquad (1)$$

Where λ is the Raman laser walength

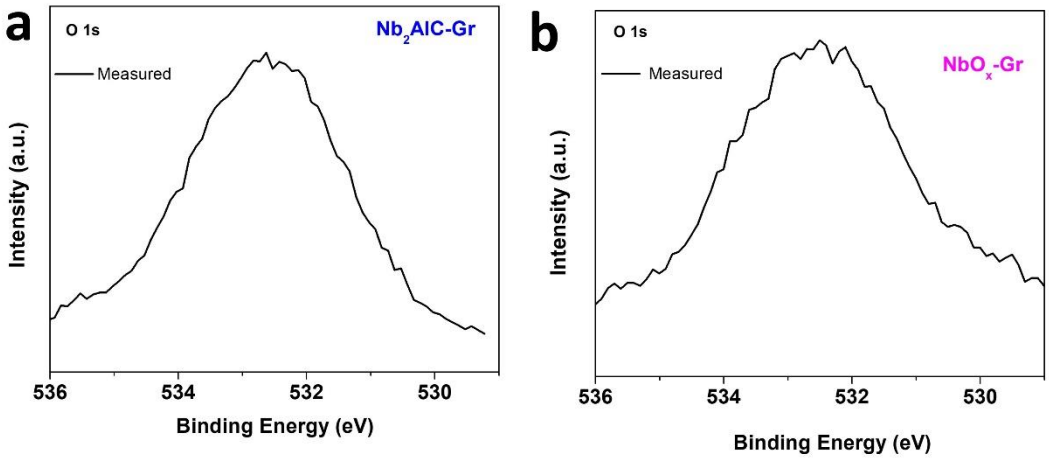

Figure S3. The high-resolution XPS spectra of O 1s for (a) Nb_2AlC-Gr, and (b) NbO_x-Gr electrodes

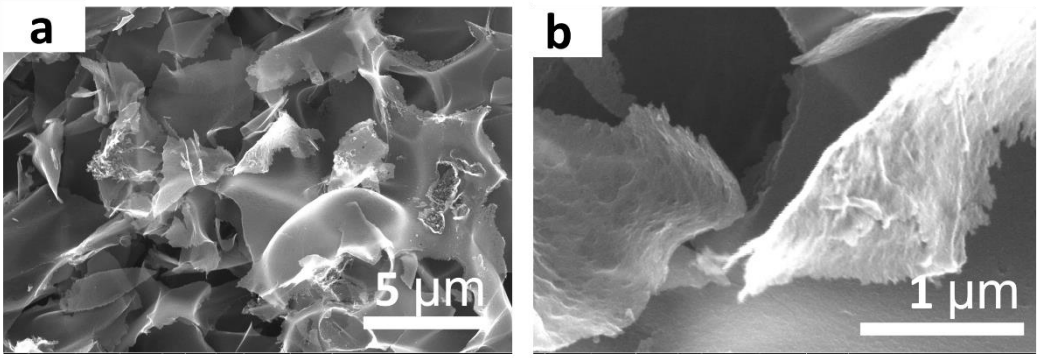

Figure S4. The SEM micrographs of laser-induced graphene (Gr); (a) low magnification and (b) high magnification.

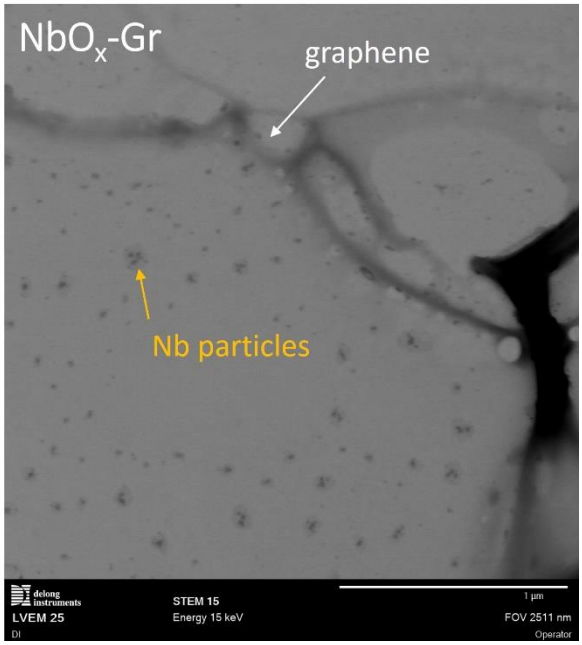

Figure S5. The STEM micrographs of NbO_x-Gr.

Electrochemical active surface area (ECSA): The electrochemical active surface area (ECSA) was calculated using the electrochemical double-layer capacitance (C_{DL}) and the specific capacitance of the carbon-based materials. The C_{DL} is calculated from the current at

various scan rates (2, 5, 7.5, and 10 mV s^{-1}) using cyclic voltammetry analysis at the non-faradic region. The linear relationship ($i_{DL} = vC_{DL}$) is followed by the scan rate (v), double-layer current (i_{DL}), and C_{DL}. Thus, the slope of double-layer current as a function of scan rate gives the value of C_{DL}. The average value of cathodic and anodic slopes is taken as the C_{DL} value.

Hence, the ECSA can be calculated using the following equation.

$$ECSA = C_{DL} / C_s ,$$

Where C_s = 22 mF cm^{-2} is the specific capacitance of the carbon-based material.[2–4]

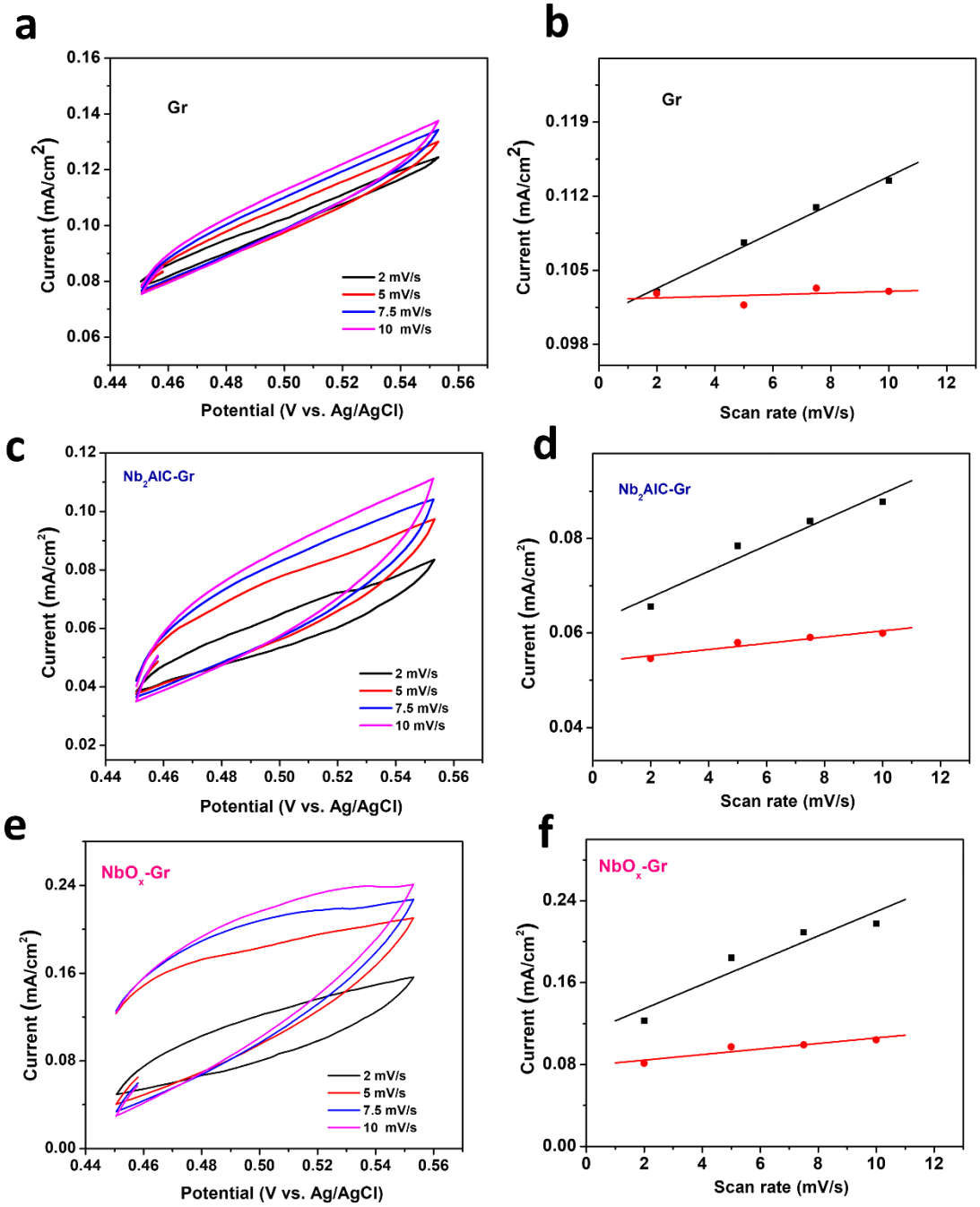

Figure S6. The electrochemical active surface area (ECSA) was calculated using cyclic voltammetry curves in the non-Faradaic region at various scan rates of the (a), (c), and (e). Gr, Nb_2AlC-Gr, and NbO_x-Gr electrodes. (b), (d), and (f). To obtain C_{DL} value, the corresponding cathodic and anodic currents from the centre of the potential region are plotted as the function of scan rate.

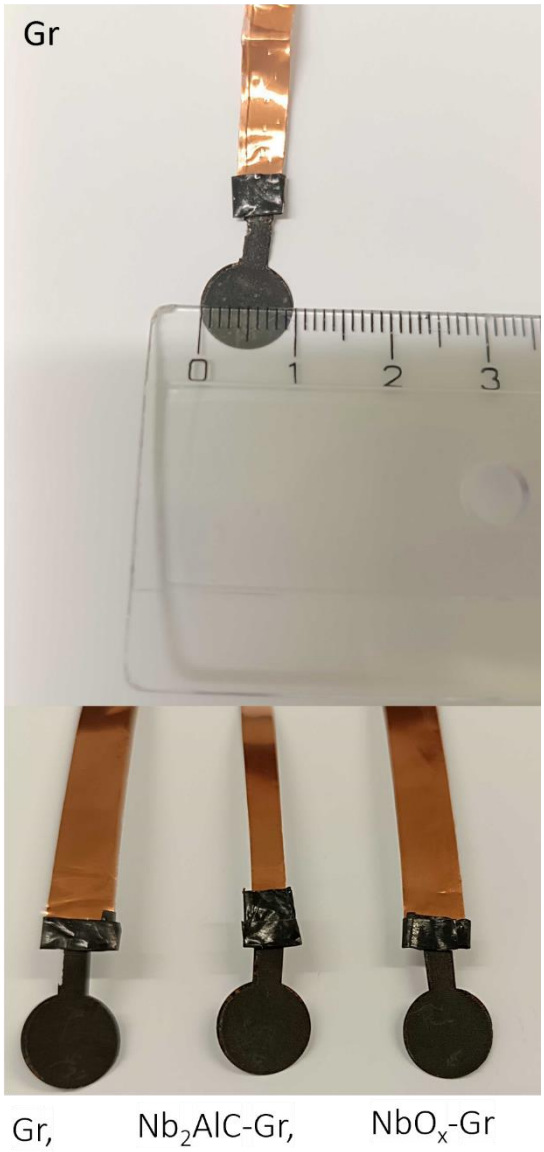

Figure S7. The images of Gr, Nb_2AlC-Gr, and NbO_x-Gr electrodes employed for nitrate reduction to ammonia generation reaction.

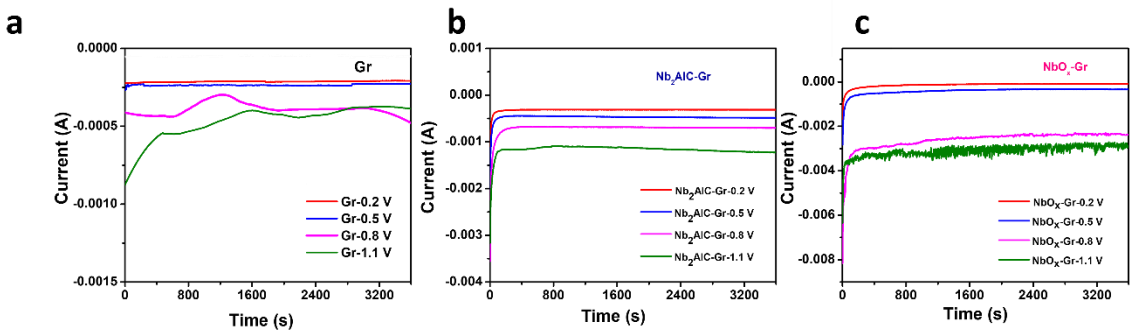

Figure S8. The chronoamperometry measurement of (a) Gr, (b) Nb_2AlC-Gr, and (c) NbO_x-Gr electrodes at different potentials.

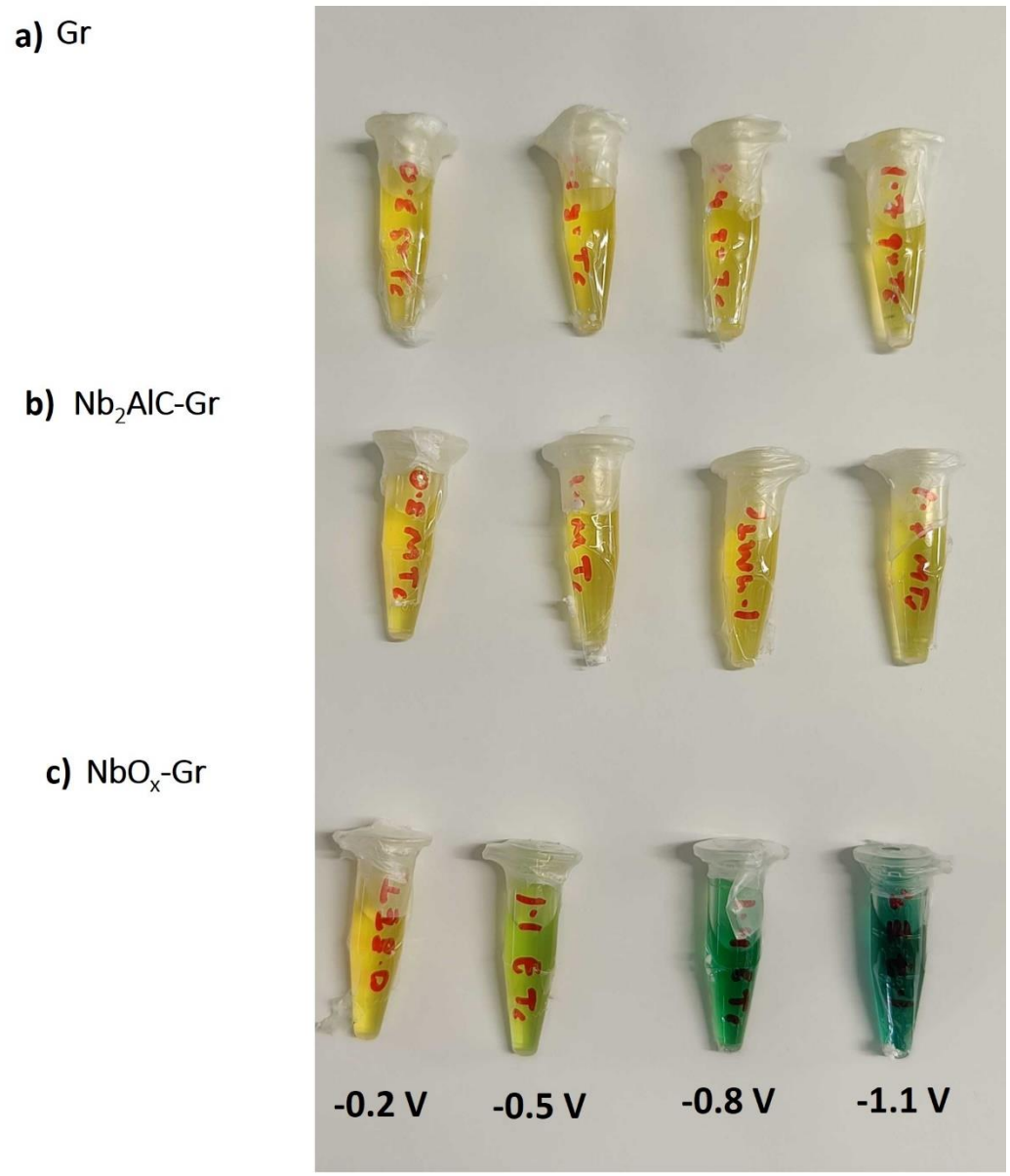

Figure S9. The electrolyte collected after electrolysis for (a) Gr, (b) Nb_2AlC-Gr, and (c) NbO_x-Gr electrodes at different potentials mixed with 600 µL (3 M NaOH, 10 wt.% salicylic acids, and 10 wt.% citric acid) 300 µL (0.2 M NaClO), and 60 µL (2.0 wt.% sodium nitroferricyanide), kept for 2 hours for ammonia detection.

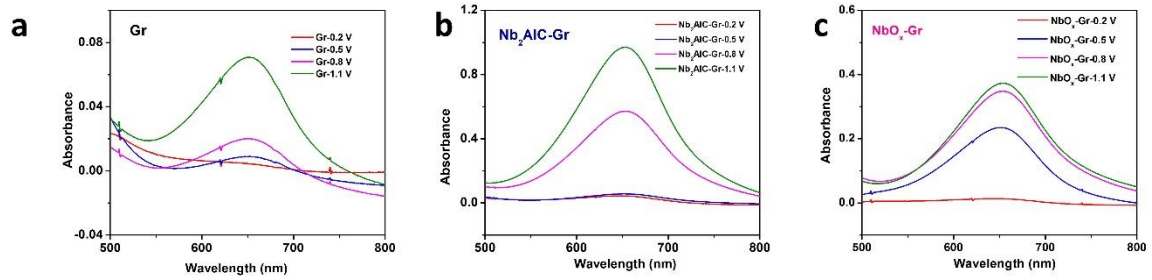

Figure S10. UV-Vis spectra of electrolysis solutions of (a) Gr, (b) Nb_2AlC-Gr, and (c) NbO_x-Gr electrodes different potentials for ammonia detection. (electrolysis solutions for -0.8 and -1.1 V diluted 7 times for NbO_x-Gr electrode).

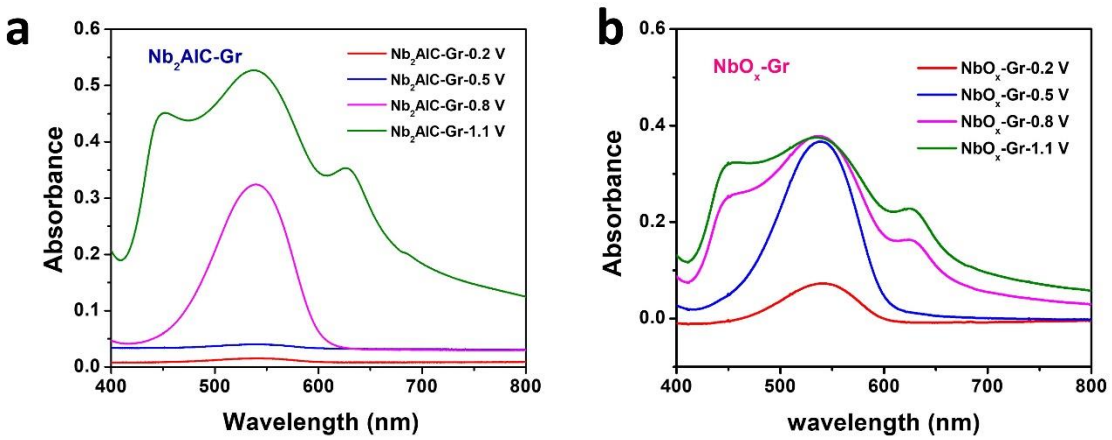

Figure S11. The UV-Vis spectra of electrolysis solutions of (a) Nb_2AlC-Gr, and (b) NbO_x-Gr electrodes at different potentials for nitrite detection. (electrolysis solutions for -0.8 and -1.1 V diluted 5 times for NbO_x-Gr electrode).

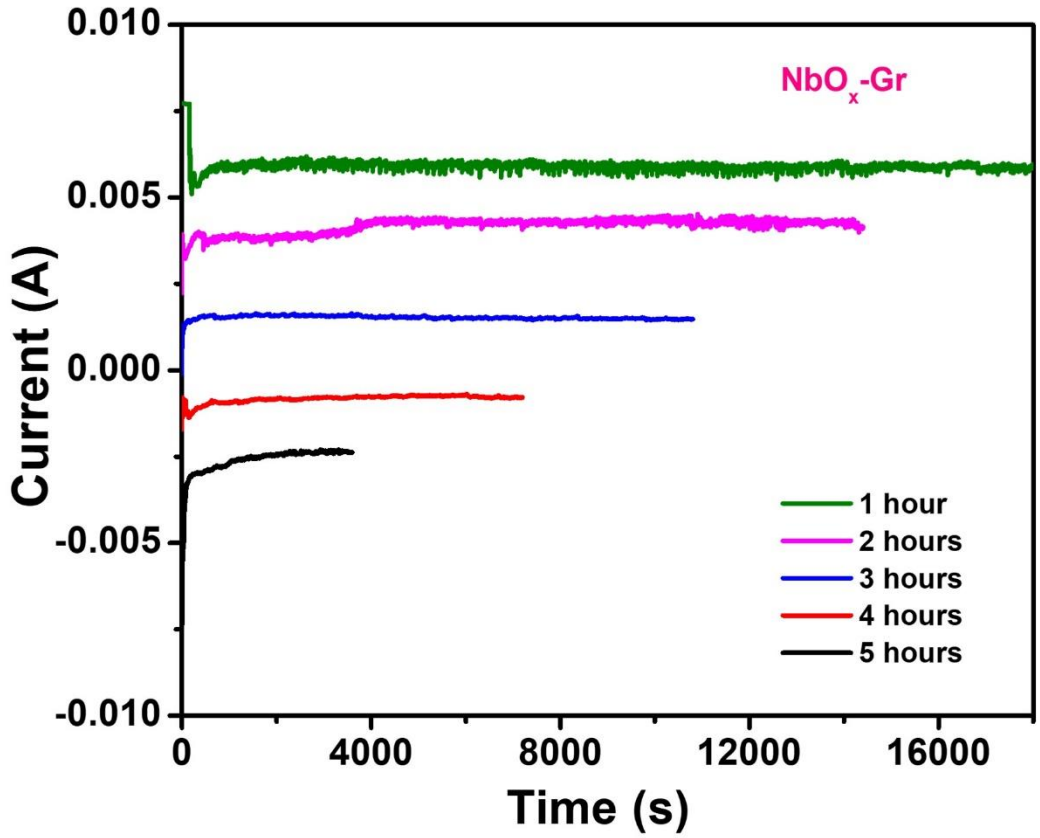

Figure S12. The ammonia generation measurement of NbO_x-Gr electrodes at a potential of -0.8 V at different times.

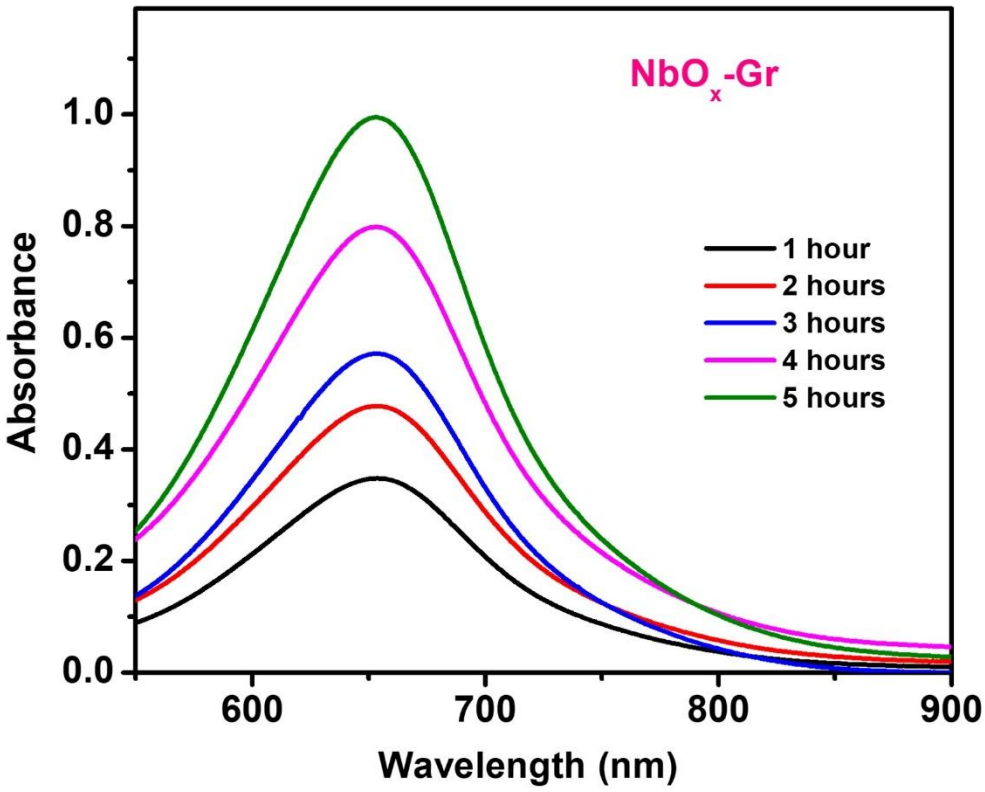

Figure S13. The UV-Vis measurement of electrolysis solutions (diluted 7 times) of NbO_x-Gr electrodes at a potential of –0.8 V.

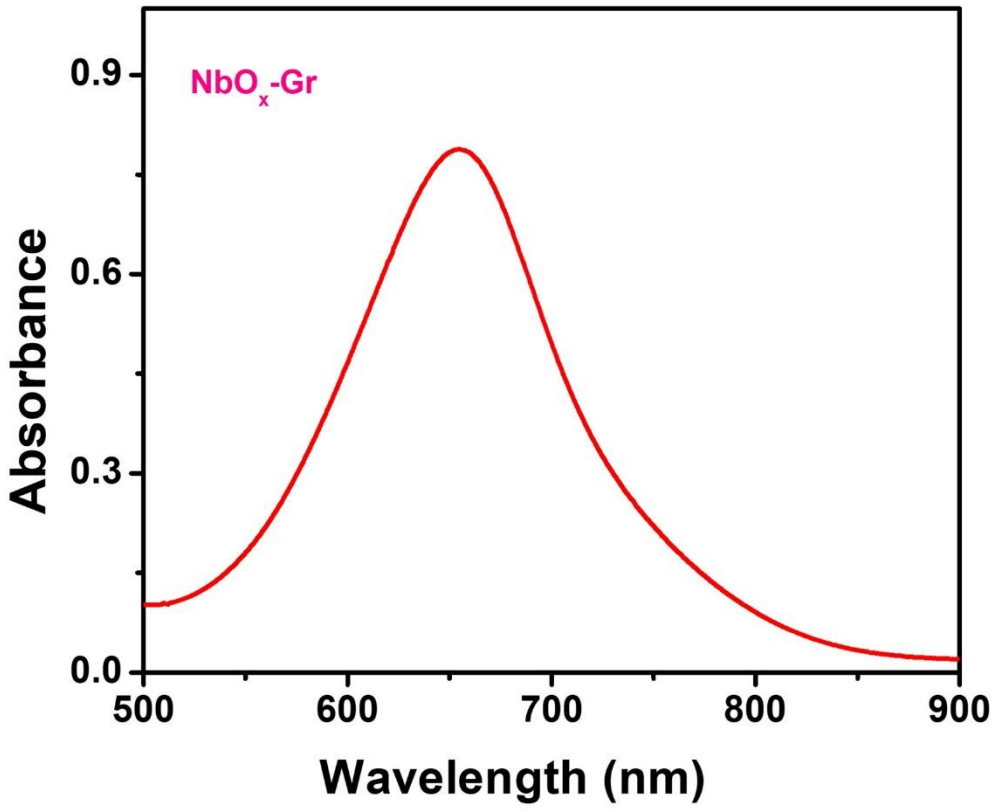

Figure S14. The UV-Vis measurement of electrolysis solutions (diluted 80 times) of NbO_x-Gr electrodes at a potential of –0.8 V for 24 hours.

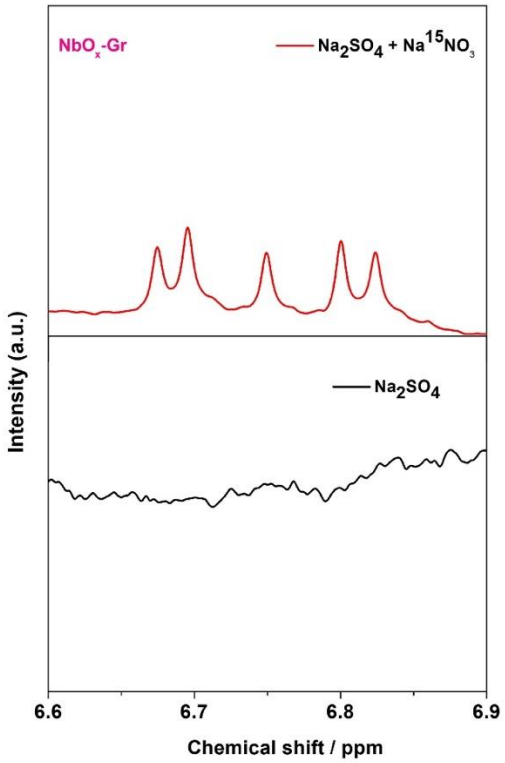

Figure S15. The ^{1}H NMR measurement of electrolysis solutions of NbO_x-Gr electrodes at a potential of –0.8 V for 2 hours in a solution of 0.5 M Na_2SO_4 + 0.1 M $Na^{15}NO_3$ (red line), compared to the blank solution 0.5 M Na_2SO_4 (black line).

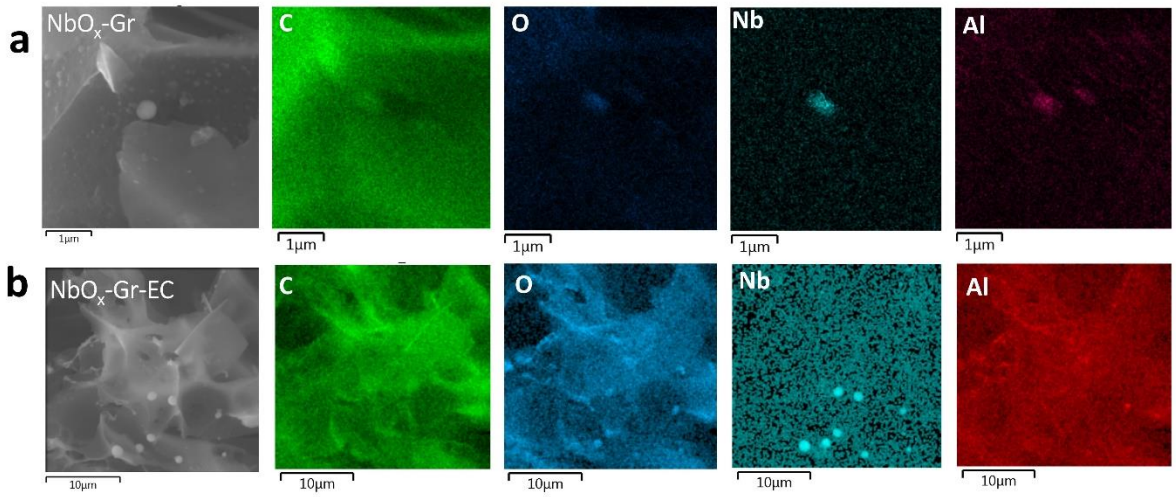

Figure S16. The SEM-EDS mapping micrographs of (a) NbO_x-Gr before elecrochemical performance and their corresponding elements like C,O, Nb, Al. (b) NbO_x-Gr-EC after elecrochemical performance and their corresponding elements like C, O, Nb, Al.

Table S1. Comparison table for nitrate reduction to ammonia with previously reported literature in recent years.

Electrocatalyst	Electrolyte	Yield rate	F.E	Potential	Ref.
MoO_2-C NBF	1 M KOH solution and 0.1 M KNO_3	≈109.28 μmol h^{-1} c m^{-2}	≈99.05 %	−0.3 V	[5]
MoO_3-C NBF	1 M KOH solution and 0.1 M KNO_3	≈22.36 μmol h^{-1} cm^{-2}	≈64.19 %	−0.3 V	[5]
Cu@Th-BPYDC	1 M KOH + 100 mM KNO_3	≈225.3 μmol h^{-1} cm^{-2}	≈92.5%	0 V *vs*. RHE	[6]
Cu@CuTCNQ	0.1 mol L^{-1} KNO_3 and 0.1 mol L^{-1} KOH	≈144.8 μmol h^{-1} cm^{-2}	≈96.4%	−0.6 V *vs*. RHE	[7]
Au nanocrystals-Co_3O_4	0.5 M KNO_3 and 1 M KOH	≈27.86 μg/h·cm^2	≈83.1%	-	[8]
MIL-101(Fe)@Nb_2C	-	≈199.68 μg h^{-1} cm^{-2}	≈89.9%	−0.3 V *vs*. RHE,	[9]
Ru–Cu/Cu_2O@Ti_3C_2	0.1 M KOH and KNO_3	≈128.35 μmol cm^{-2} h^{-1}	≈48.3%	−0.7 V *vs*. RHE	[10]
Mo_2CT_x : Fe	0.05 M H_2SO_4, 100 mM NO_3^- (from $NaNO_3$)	≈3.2 μmol h^{-1} mg^{-1},	≈41 %	−0.4 V *vs*. RHE	[11]

Mo_2CT_x : Fe	0.5 M Na_2SO_4 100 mM NO_3	≈12.9 μmol h^{-1} mg^{-1}	≈70 %	-	[11]
FeSA/MXene	0.1 mol L^{-1} Na_2SO_4 and $NaNO_3$ (50 mg-N L^{-1})	-	≈82.9	−1.4 V (*vs* Ag/AgCl)	[12]
a1-Ru/CNTs	500 ppm NO3 -	≈145.1 μg·h -1·mgcat. -1	≈80.62	−0.2 V vs RHE	[13]
Pd/NF	0.5 M Na_2SO_4 with 0.1 M $NaNO_3$	≈1.52 mmol cm^{-2} h^{-1}	≈ 78	−1.4 V versus RHE	[14]
FOSP-Cu-0.1	0.5 M Na_2SO_4 with 0.1 M $NaNO_3$	101.4 μmol h^{-1} cm^{-2}	93.91	− 0.266 V vs. RHE,	[15]
Co-NAs	1 M KOH with 0.1 M NO_3^-	10.4 mmol h^{-1} cm^{-2}	-	−0.24 V	[16]
GB Ni NPs	1 M $NaNO_3$ + 1 M NaOH	15.49 mmol h^{-1} cm^{-2}	93.0%	−0.93 V,	[17]
Bi/Pd	1 M KOH with and 0.1 M NO_3^-.	33.8 mg h^{-1} cm^{-2}	100	−0.6 V versus RHE	[18]
$Cu_{0.65}Pd_{0.35}O_x$	0.1 M KNO_3	1.41 mg h^{-1} cm^{-2}	-	$-0.2\ V_{RHE}$	[19]
CuCoSP	0.1 M NO_3^-	1.17 mmol cm^{-2} h	93.3 ± 2.1	−0.175 V vs. RHE	[20]
MoO_2-C NBF	1 M KOH with 0.1 M KNO_3	109.28 μmol h^{-1} cm^{-2}	99.05	−0.3 V vs RHE	[21]
Gr	0.5 M Na_2SO_4 with 0.1M KNO_3	≈5.68 μg h^{-1} cm^{-2}	≈ 9.05	−1.1 V *vs.* RHE	This work
Nb_2AlC-Gr	0.5 M Na_2SO_4 with 0.1M KNO_3	≈ 71.50 μg h^{-1} cm^{-2}	≈ 45.47	−1.1 V *vs.* RHE	This work
NbO_x-Gr electrodes	0.5 M Na_2SO_4 with 0.1M KNO_3	≈ 194.79 μg h^{-1} cm^{-2}	≈ 46.50	−1.1 V *vs.* RHE	This work

Binding energy calculation:

The binding energy of the NbOx model on graphene was calculated using DFT calculations (equation 2), introducing the projector augmented wave (PAW) potential with a plane-wave cutoff energy of 520 eV. The Perdew-Burke-Enrzerhof (PBE) parametrization of the generalized gradient approximation (GGA) was used to describe the electronic exchange-correlation energies, and DFT-D3 method of Grimme with zero-damping was also introduced to describe the van der Waals interactions.

$$E_{\text{bind}} = E_{\text{complex}} - E_{\text{NbOx}} - E_{\text{graphene}} \quad (2)$$

where E_{complex} is the total energy of NbO_x-Gr system, E_{NbOx} energy of an isolated NbO_x nanocluster, and E_{graphene} energy of an isolated graphene sheet, all being in the geometry of the NbO_x-Gr system.

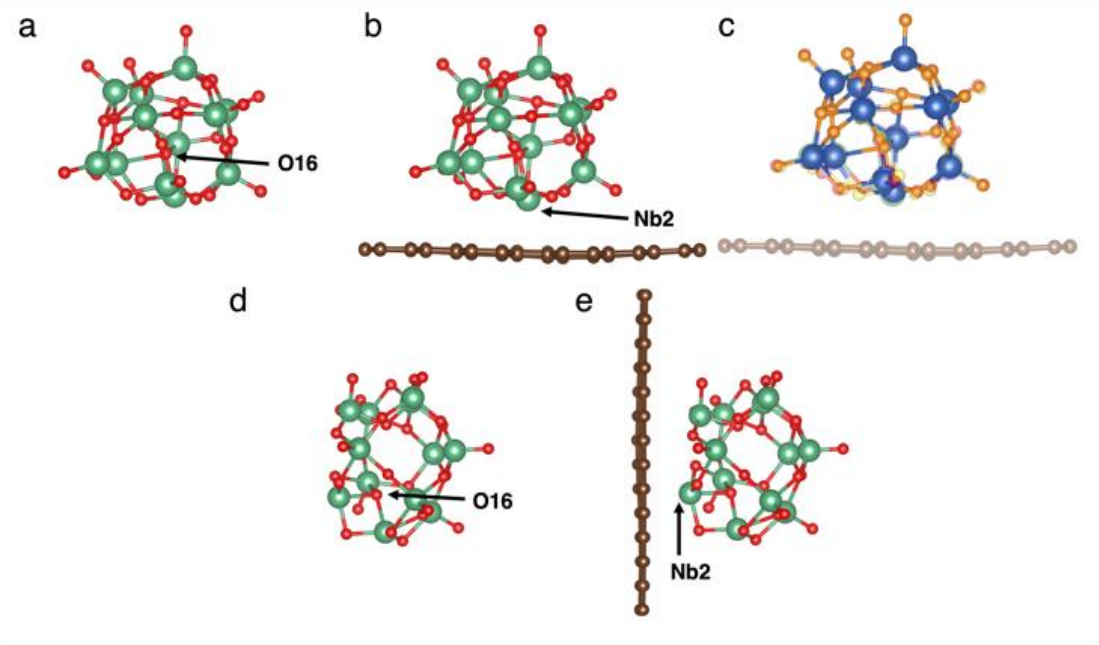

Figure S17. Graphical representation of structural changes of the NbO_x nanocluster before (a, d) and after (b, e) adsorption on graphene. Panel (c) shows overlayed panels (a) and (b) for comparison. Label: O16 and Nb2 are identified as the atoms exhibiting the most significant change in bond length.

Table S2: Interatomic bond distances (in Å) in the NbO_x model before (top half) and after (bottom half) adsorption on graphene. Changes in bond lengths after adsorption are relative to the pre-adsorption values.

No graphene support																													
	O1	O2	O3	O4	O5	O6	O7	O8	O9	O10	O11	O12	O13	O14	O15	O16	O17	O18	O19	O20	O21	O22	O23	O24	O25	O26	O27	O28	O29	O30
Nb1	1.96	1.75	1.89								2.01																			
Nb2				1.88			1.80					1.93				1.97														
Nb3	1.96				1.73			2.11					2.03				2.14													
Nb4			2.06			1.98	2.21			1.73				1.98																
Nb5								1.87			1.91				1.88		2.36			1.99										
Nb6						1.93									2.03			1.74					1.90							
Nb7				2.07					1.73				1.87			2.43					2.09									
Nb8												2.00				2.03			1.86							1.90		2.12		
Nb9																	1.92			2.10	2.10			2.07			1.74			
Nb10														1.92					2.14			1.74			1.97			2.20		
Nb11																				2.30			1.98	2.11	1.90				1.73	
Nb12																					2.13			2.07		2.06		1.97		1.73

With graphene support																														
	O1	O2	O3	O4	O5	O6	O7	O8	O9	O10	O11	O12	O13	O14	O15	O16	O17	O18	O19	O20	O21	O22	O23	O24	O25	O26	O27	O28	O29	O30
Nb1	-0.04	0.00	-0.02								0.00																			
Nb2				-0.07			0.00					-0.02				-0.16														
Nb3	0.03				-0.01			-0.01					0.00				0.00													
Nb4			0.04			0.01	0.00			-0.01				0.02																
Nb5								0.01			0.01				-0.01		0.01			-0.01										
Nb6						0.01									0.01			0.00					0.00							
Nb7				0.02					-0.01				-0.02			0.13					0.00									
Nb8												0.03				0.07			0.00							0.00		-0.11		
Nb9																	-0.01			-0.01	0.00			0.02			0.00			
Nb10														-0.01					0.01			0.00			-0.02			0.05		
Nb11																				-0.01			-0.01	0.01	0.00				-0.01	
Nb12																					-0.01			-0.03		0.00		0.04		-0.01

References

(1) Li, W.; Peng, D.; Huang, W.; Zhang, X.; Hou, Z.; Zhang, W.; Lin, B.; Xing, Z. Adjusting Coherence Length of Expanded Graphite by Self-Activation and Its Electrochemical Implication in Potassium Ion Battery. *Carbon N Y* **2023**, *204*, 315–324. https://doi.org/10.1016/j.carbon.2022.12.072.

(2) Mccrory, C. C. L.; Jung, S.; Peters, J. C.; Jaramillo, T. F. *Benchmarking Heterogeneous Electrocatalysts for the Oxygen Evolution Reaction*.

(3) Gao, W.; Iffelsberger, C.; Pumera, M. Dual Polymer Engineering Enables High-Performance 3D Printed Zn-Organic Battery Cathodes. *Appl Mater Today* **2022**, *28*. https://doi.org/10.1016/j.apmt.2022.101515.

(4) Gao, W.; Perales-Rondon, J. V.; Michalička, J.; Pumera, M. Ultrathin Manganese Oxides Enhance the Electrocatalytic Properties of 3D Printed Carbon Catalysts for Electrochemical Nitrate Reduction to Ammonia. *Appl Catal B* **2023**, 122632. https://doi.org/10.1016/j.apcatb.2023.122632.

(5) Yan, J.; Liu, P.; Li, J.; Huang, H.; Song, W. Effect of Valence State on Electrochemical Nitrate Reduction to Ammonia in Molybdenum Catalysts. *Chemical Engineering Journal* **2023**, *459*, 141601. https://doi.org/10.1016/j.cej.2023.141601.

(6) Gao, Z.; Lai, Y.; Tao, Y.; Xiao, L.; Zhang, L.; Luo, F. Constructing Well-Defined and Robust Th-MOF-Supported Single-Site Copper for Production and Storage of Ammonia

from Electroreduction of Nitrate. *ACS Cent Sci* **2021**, *7* (6), 1066–1072. https://doi.org/10.1021/acscentsci.1c00370.

(7) Zhou, N.; Wang, J.; Zhang, N.; Wang, Z.; Wang, H.; Huang, G.; Bao, D.; Zhong, H.; Zhang, X. Defect-Rich Cu@CuTCNQ Composites for Enhanced Electrocatalytic Nitrate Reduction to Ammonia. *Chinese Journal of Catalysis* **2023**, *50*, 324–333. https://doi.org/10.1016/S1872-2067(23)64454-7.

(8) Zhang, M.; Song, K.; Liu, C.; Zhang, Z.; He, W.-Q.; Huang, H.; Liu, J. Electron-Rich Au Nanocrystals/Co3O4 Interface for Enhanced Electrochemical Nitrate Reduction into Ammonia. *J Colloid Interface Sci* **2023**, *650*, 193–202. https://doi.org/10.1016/j.jcis.2023.06.073.

(9) Zhu, H.; Xue, S.; Zhao, F.; Hua, Q.; Liang, Z.; Ren, X.; Gao, L.; Ma, T.; Liu, A. MIL-101(Fe)@Nb $_2$ C MXene for Efficient Electrocatalytic Ammonia Production: An Experimental and Theoretical Study. *New Journal of Chemistry* **2023**, *47* (32), 15302–15308. https://doi.org/10.1039/D3NJ02436A.

(10) Zhao, F.; Li, G.; Hua, Q.; Cao, J.; Song, J.; Gao, L.; Ma, T.; Ren, X.; Liu, A. A Two-Dimensional MXene-Supported CuRu Catalyst for Efficient Electrochemical Nitrate Reduction to Ammonia. *Catal Sci Technol* **2023**, *13* (19), 5543–5548. https://doi.org/10.1039/D3CY01009K.

(11) Abbott, D. F.; Xu, Y.; Kuznetsov, D. A.; Kumar, P.; Müller, C. R.; Fedorov, A.; Mougel, V. Understanding the Synergy between Fe and Mo Sites in the Nitrate Reduction Reaction on a Bio-Inspired Bimetallic MXene Electrocatalyst. *Angewandte Chemie International Edition* **2023**, *62* (51). https://doi.org/10.1002/anie.202313746.

(12) Ren, Y.; Tian, F.; Jin, L.; Wang, Y.; Yang, J.; You, S.; Liu, Y. Fluidic MXene Electrode Functionalized with Iron Single Atoms for Selective Electrocatalytic Nitrate Transformation to Ammonia. *Environ Sci Technol* **2023**, *57* (28), 10458–10466. https://doi.org/10.1021/acs.est.3c02520.

(13) Jiang, M.; Tao, A.; Hu, Y.; Wang, L.; Zhang, K.; Song, X.; Yan, W.; Tie, Z.; Jin, Z. Crystalline Modulation Engineering of Ru Nanoclusters for Boosting Ammonia Electrosynthesis from Dinitrogen or Nitrate. *ACS Appl Mater Interfaces* **2022**, *14* (15), 17470–17478. https://doi.org/10.1021/acsami.2c02048.

(14) Guo, H.; Li, M.; Yang, Y.; Luo, R.; Liu, W.; Zhang, F.; Tang, C.; Yang, G.; Zhou, Y. Self-Supported Pd Nanorod Arrays for High-Efficient Nitrate Electroreduction to Ammonia. *Small* **2023**, *19* (10). https://doi.org/10.1002/smll.202207743.

(15) Zhao, Y.; Liu, Y.; Zhang, Z.; Mo, Z.; Wang, C.; Gao, S. Flower-like Open-Structured Polycrystalline Copper with Synergistic Multi-Crystal Plane for Efficient Electrocatalytic Reduction of Nitrate to Ammonia. *Nano Energy* **2022**, *97*, 107124. https://doi.org/10.1016/j.nanoen.2022.107124.

(16) Deng, X.; Yang, Y.; Wang, L.; Fu, X.; Luo, J. Metallic Co Nanoarray Catalyzes Selective NH_3 Production from Electrochemical Nitrate Reduction at Current Densities Exceeding 2 A Cm^{-2}. *Advanced Science* **2021**, *8* (7). https://doi.org/10.1002/advs.202004523.

(17) Zhou, J.; Wen, M.; Huang, R.; Wu, Q.; Luo, Y.; Tian, Y.; Wei, G.; Fu, Y. Regulating Active Hydrogen Adsorbed on Grain Boundary Defects of Nano-Nickel for Boosting Ammonia Electrosynthesis from Nitrate. *Energy Environ Sci* **2023**, *16* (6), 2611–2620. https://doi.org/10.1039/D2EE04095F.

(18) Chen, K.; Ma, Z.; Li, X.; Kang, J.; Ma, D.; Chu, K. Single-Atom Bi Alloyed Pd Metallene for Nitrate Electroreduction to Ammonia. *Adv Funct Mater* **2023**, *33* (12). https://doi.org/10.1002/adfm.202209890.

(19) Jung, W.; Jeong, J.; Chae, Y.; Lee, W. H.; Ko, Y.-J.; Chae, K. H.; Oh, H.; Lee, U.; Lee, D. K.; Min, B. K.; Shin, H.; Hwang, Y. J.; Won, D. H. Synergistic Bimetallic CuPd Oxide Alloy Electrocatalyst for Ammonia Production from the Electrochemical Nitrate Reaction. *J Mater Chem A Mater* **2022**, *10* (44), 23760–23769. https://doi.org/10.1039/D2TA06316F.

(20) He, W.; Zhang, J.; Dieckhöfer, S.; Varhade, S.; Brix, A. C.; Lielpetere, A.; Seisel, S.; Junqueira, J. R. C.; Schuhmann, W. Splicing the Active Phases of Copper/Cobalt-Based Catalysts Achieves High-Rate Tandem Electroreduction of Nitrate to Ammonia. *Nat Commun* **2022**, *13* (1), 1129. https://doi.org/10.1038/s41467-022-28728-4.

(21) Yan, J.; Liu, P.; Li, J.; Huang, H.; Song, W. Effect of Valence State on Electrochemical Nitrate Reduction to Ammonia in Molybdenum Catalysts. *Chemical Engineering Journal* **2023**, *459*, 141601. https://doi.org/10.1016/j.cej.2023.141601.